ACS APPLIED MATERIALS & INTERFACES

Research Article

www.acsami.org

Highly Efficient and Selective Oxidation of Aromatic Alcohols Photocatalyzed by Nanoporous Hierarchical Pt/Bi_2WO_6 in Organic Solvent-Free Environment

M. Qamar,*[,†] Rami B. Elsayed,[‡] Khalid R. Alhooshani,[‡] Muhammad I. Ahmed,[†] and Detlef W. Bahnemann*[,§]

[†]Center of Excellence in Nanotechnology (CENT), [‡]Department of Chemistry, King Fahd University of Petroleum and Minerals, Dhahran 31261, Kingdom of Saudi Arabia

[§]Institut fuer Technische Chemie, Leibniz Universität Hannover, Callinstrasse 3, D-30167 Hannover, Germany

Supporting Information

ABSTRACT: Selective conversion of aromatic alcohols into corresponding aldehydes is important from energy and environmental stance. Here, we describe highly selective (>99%) and efficient conversion (>99%) of aromatic alcohols (e.g., 4-methoxybenzyl alcohol and 4-nitrobenzyl alcohol) into their corresponding aldehydes in the presence of Pt-modified nanoporous hierarchical Bi_2WO_6 spheres in water under simulated sunlight at ambient conditions. Overoxidation of *p*-anisaldehyde, formed during photooxidation process, was not observed until comprehensive alcohol oxidation was attained. Furthermore, the catalyst showed substantial oxidation under dark and course of conversion was different than that of under light. Dependency of alcohol oxidation on substrate concentration, photocatalyst amount, and Pt loading was studied. The effect of various radical scavengers was investigated, and the rate-determining step was elucidated. It has been envisaged that the reduction site of semiconductor photocatalysts plays more decisive role in determining the selectivity as alcohol preferably get oxidized over that of water. Furthermore, the chemical stability and recyclability of the photocatalyst were investigated.

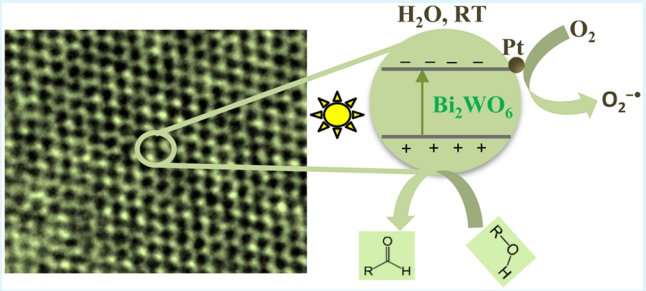

KEYWORDS: *bismuth tungstate (Bi_2WO_6), semiconductor photocatalyst, heterogeneous catalysis, alcohol oxidation, sunlight*

1. INTRODUCTION

Oxidation of alcohols into aldehydes is one of the indispensable transformations in organic synthesis as aldehydes are widely used in food, beverages, and pharmaceutical industries, and as precursors in chemical industries.[1,2] From environmental and energy viewpoints, oxidation of alcohols in water under ambient conditions is exigent, but notable progress remains to be achieved. In the conventional processes, although several metal-based reagents have been developed that can selectively and efficiently oxidize alcohols, the requirement of stoichiometric amounts of the metal oxidants and accumulation of a considerable amount of waste remain inevitable.[1,3] Moreover, reactions are customarily carried out in organic solvents to achieve high selectivity toward products. To the contrary, the utilization of heterogeneous semiconductor-mediated photocatalytic process, which utilizes abundant sunlight, relatively inexpensive and nontoxic photocatalysts, for such synthesis transformations seems propitious owing to its renewable attributes. Yet, the photocatalytic process in context of selective oxidation is still in its infancy as photocatalysts are being researched to induce selective organic functional group transformations. The fundamentals of semiconductor-mediated photocatalytic process have been well documented in the literature by a multitude of authors.[4−6] Briefly, by providing energy equal to or greater than the band gap of semiconductor photocatalyst, an electron may be promoted from the valence band to the conduction band (e^-cb) leaving behind an electron vacancy or "hole" in the valence band (h^+vb). If the charge separation is maintained, the electron and hole may migrate to the catalyst surface where they participate in redox reactions with absorbed species. Specially, h^+vb may oxidize surface-bound H_2O or OH^- to produce hydroxyl radical ($OH^•$), and e^-cb can reduce oxygen to generate superoxide radical anion ($O_2^{-•}$). These radical species are extremely reactive and make the photocatalytic process somewhat nonselective. Due to its nonselective attributes, most of the previous studies involving photocatalysis focused on environmental cleanup, H_2 production, and CO_2 reduction, etc.[4−8] Recently, the perspectives of photocatalytic process for the synthesis of fine chemicals in energy efficient and environmentally benign pathway have been envisaged and numerous photocatalysts are being explored.[9−11] Some of the photocatalysts investigated for alcohol oxidation

Received: October 26, 2014
Accepted: December 23, 2014
Published: December 23, 2014

DOI: 10.1021/am507428r
ACS Appl. Mater. Interfaces 2015, 7, 1257−1269

include CdS/graphene,[12] CdS/graphene/TiO_2,[13] and pristine (rutile,[14−17] anatase,[18] and brookite[19]) as well as surface-modified titania (Nb_2O_5/TiO_2,[20] Pt/TiO_2,[21] transition metals/TiO_2,[22]). Although encouraging results have been reported, the challenge of selectivity together with high efficiency remains to be addressed. For instance, on one hand, selective and complete oxidation of benzyl alcohol to benzaldehyde was achieved in aqueous suspensions of Au/CeO_2, but the reaction rate was rather low for benzaldehyde formation (~3.0 μmol h^{-1}).[23,24] On the other hand, the rutile form of TiO_2 was demonstrated to be highly efficient photocatalyst for the oxidation of alcohols, selectivity remained a major concern as the overoxidation of byproducts was observed.[14] Moreover, TiO_2 is active only in the ultraviolet region. Thus, development of photocatalysts that operate under visible region and can selectively and efficiently drive the oxidation of alcohols in water under mild conditions remains an attractive challenge. The challenge could be addressed by designing or selecting photocatalyts with appropriate band edges. To this end, Bi_2WO_6 appears to be a promising visible-light-driven photocatalyst owing to its high photocatalytic efficiency.[25−29] Further, more importantly, the stability and recyclability of Bi_2WO_6 under photocatalytic conditions have been shown to be excellent.[30−32] Recently, bismuth tungstate has been identified as a visible-light-driven photocatalyst for highly chemoselective conversion of glycerol.[33] Xue et al. reported the selective conversion of glycerol into dihydroxyacetone; 96% conversion of glycerol was achieved with ~91% selectivity and ~87% yield after 5 h irradiation. Although high selectivity and yield was achieved, the conversion rate was observed to be extremely low (ca. 20 μmol h^{-1}) in the presence of high amount of Bi_2WO_6 (>5 g L^{-1}).

Since the photocatalytic processes are largely a surface-dictated phenomena, the challenge of low conversion rate could be addressed by engineering the surface of bismuth tungstate and incorporating active functionalities. Among various surface engineering strategies, generating porosity on the surface appears propitious, in particular, because it provides sufficient surface area for the adsorption of reactants and faster migration or diffusion of the parent as well as intermediate products, thereby augmenting the overall efficiency of the catalytic process.

In the study presented here, it is demonstrated that the efficiency of selective conversion of alcohols could be significantly improved by developing Bi_2WO_6 with nanoporous surface and hierarchical morphology, in addition to incorporation of Pt. Platinum was deposited onto the surface of Bi_2WO_6 to preclude intrinsic but unsought electron−hole pair recombination, which remains more ubiquitous in the absence of oxidant. Selectivity and efficiency of Pt/nanoporous Bi_2WO_6 were demonstrated by studying the conversion of representative aromatic alcohols namely 4-methoxybenzyl alcohol and 4-nitrobenzyl alcohol.

2. EXPERIMENTAL SECTION

2.1. Synthesis of Nanoporous Hierarchical Bi_2WO_6. In a typical synthesis, 0.5 g Pluronic F127 was completely dissolved in 20 mL water acidified with nitric acid (pH ~ 1). Bismuth nitrate (0.08 M) was added and the solution was stirred until a clear solution was obtained. On the other hand, an aqueous solution of sodium tungstate (0.04 M, 20 mL of water) was prepared separately. Solution of sodium tungstate was added dropwise to the mixture of bismuth nitrate with vigorous stirring at room temperature. As a result, a white colloidal solution was obtained, which was further kept under stirring for 2 h. Then, the solution was transferred into a 125 mL Teflon vessel and heated at 170 °C for 20 h under autogenous pressure. After cooling, the product was collected, thoroughly washed with ethanol (80 °C for several hours) to remove any residual surfactant, and dried at 110 °C under vacuum overnight. Synthesis of nonporous Bi_2WO_6 was carried out following the above-described synthesis steps except the addition of Pluronic PF127.

2.2. Synthesis of Pt/Nanoporous Bi_2WO_6. The deposition of platinum onto the surface of the Bi_2WO_6 was performed using a photodeposition method in a similar immersion well photochemical reactor (Supporting Information Figure S8). Briefly, 130 mL of water was added to the reaction vessel and the required amounts of metal salt (H_2PtCl_6) and Bi_2WO_6 were added. The suspension was stirred and purged with high purity argon gas for at least 1 h to remove the dissolved oxygen. Methanol (10 vol %) was added as an electron donor. Irradiation was carried out using a 230 W tungsten−halogen lamp (OSRAM) for 6 h. After irradiation, the Pt loaded catalyst was washed with water and ethanol and separated through centrifugation and dried at 110 °C under vacuum overnight. Synthesis of Pt/nonporous Bi_2WO_6 was also carried out following the above-described deposition method, except that nonporous Bi_2WO_6 was utilized instead of nanoporous Bi_2WO_6.

2.3. Characterization. Characterization was carried out by employing high-resolution transmission electron microscopy (HR-TEM), high-angle annular dark-field transmission electron microscopy (HAAD-TEM), field emission scanning electron microscopy (FESEM), energy dispersive X-ray spectroscopy (EDS), X-ray diffractometer (XRD), Fourier transform infrared spectroscopy (FTIR), BET surface area analyzer, diffuse reflectance spectroscopy (DRS).

2.4. Photocatalytic Experiments. The photocatalytic activity for oxidation of alcohols was evaluated using immersion well photochemical reactor made of Pyrex glass equipped with a magnetic stirring bar, a water circulating jacket and with openings for supply of gases. A detailed schematic of photocatalytic reactor is delineated in Supporting Informationi Figure S8. For irradiation experiment, 130 mL solution was taken into the photoreactor and required amount of photocatalyst was added, and the solution was stirred for at least 15 min in the dark. The zero time reading was obtained from the solution withdrawn before the light was turned on. Irradiations were carried out using a 230 W tungsten-halogen lamp (OSRAM), which emits <2% UV light, a radiation spectrum emulating sunlight. The temperature was controlled and kept at room temperature by circulating cold water through the outer jacket of the reactor. Samples (3 mL) were collected before and at regular intervals during the irradiation, and the catalyst was removed by filtration.

2.5. GC-MS Analysis. All the irradiated solutions were extracted with 3 mL of chloroform in three portions, 1 mL each, for maximum extraction. Analysis of the extracted samples was carried out by gas chromatography mass spectrometer (Agilent Technologies) using capillary column (5% phenyl methyl siloxan, 30 m × 320 μm × 0.25 μm). Selected ion monitoring mode (SIM) was used for routine analysis. Programing of the GC oven temperature was as follows: it was set to reach 40 °C in 1 min, then 10 °C/min to reach 200 °C. Injection volume was 100 nL with split ratio 2:1. The calibration curves were obtained by injecting standards solutions of reactants and products, such as benzyl alcohol, benzaldehyde, 4-methoxy benzyl alcohol, 4-methoxy benzaldehyde, and so on. The concentrations of alcohols and aldehydes were determined from the peak areas. Percent (%) conversion, selectivity, and yield were calculated using the following formulas:

$$\text{Selectivity} = \frac{C_p}{(C_{r_0} - C_r)} 100$$

$$\%\ \text{Conversion} = \frac{(C_{r_0} - C_r)}{C_{r_0}} 100$$

DOI: 10.1021/am507428r
ACS Appl. Mater. Interfaces 2015, 7, 1257−1269

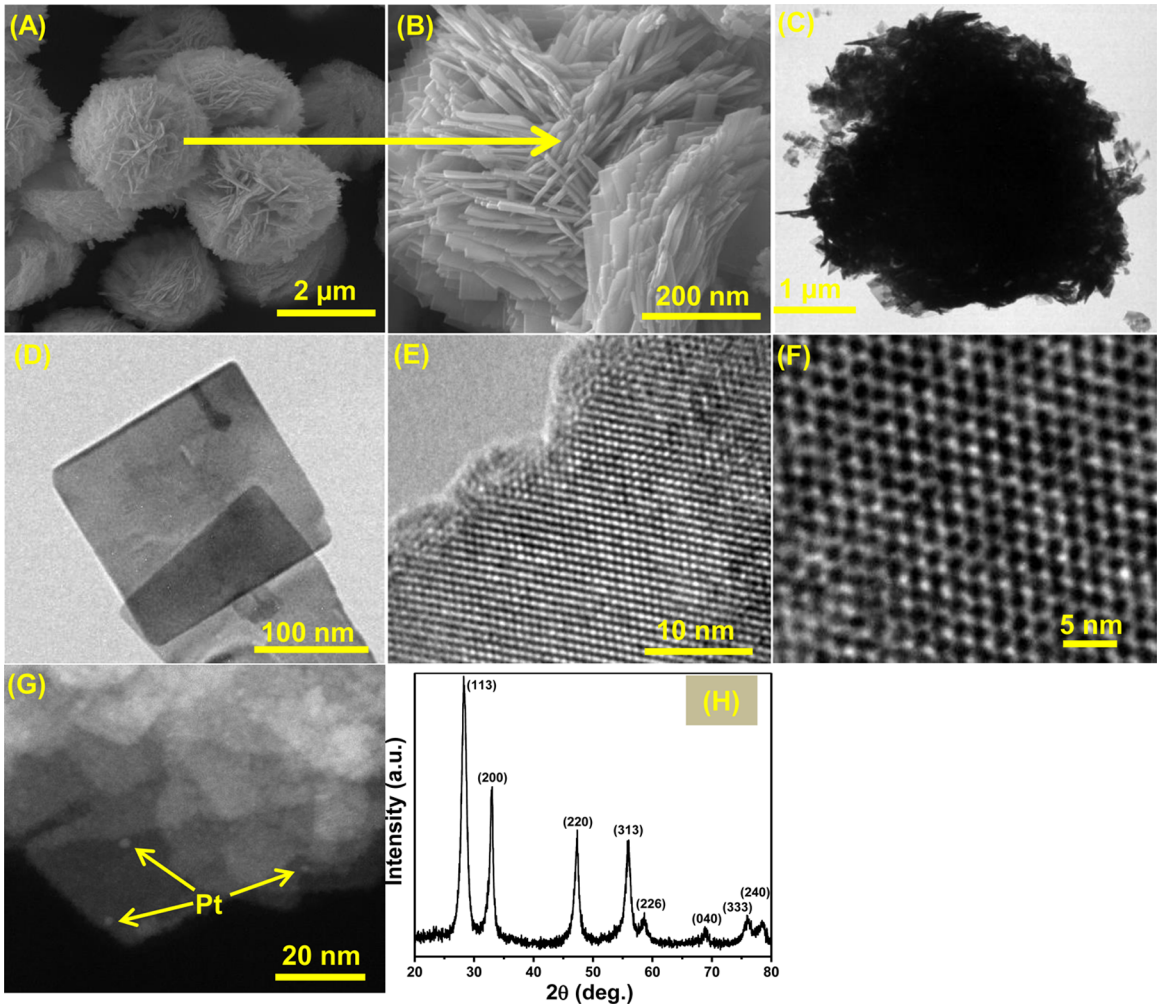

Figure 1. (A and B) FESEM, (C–F) TEM and HRTEM, (G) HAAD-TEM, and (H) XRD of platinized nanoporous Bi_2WO_6.

$$\% \text{ Yield} = \frac{C_p}{C_{r_0}} 100$$

C_{r_0} = the initial concentration of the reactant, C_r = the concentration of the reactant during the reaction, C_p = the concentration of the product during the reaction.[34]

2.6. Photoluminescence Studies. 120 mL of the 5×10^{-4} M terephthalic acid aqueous solution with concentration of 2×10^{-3} M NaOH was taken into the photoreactor. Reactions were carried out both in the absence or presence of 1×10^{-3} M 4-MBA. The required amount of photocatalyst was added, and the resulting suspension was kept under stirring for 15 min under dark. Then, the lamp was turned on and samples were collected and filtered to remove catalyst particles. Photoluminescence analysis of irradiated solutions was performed on a fluorescence spectrophotometer (Horiba, FluoroLog-3) using an excitation wavelength of 308 nm.

2.7. In Situ ATR-FTIR Study. In situ ATR-FTIR measurements were performed on Thermo Nicolet FTIR spectrophotometer equipped with horizontal smart *i*TR accessory (diamond-faced ZnSe prism). The top surface of ATR crystal was properly covered with the photocatalyst (~5 mg) and 25 μL solution of 4-MBA (with 1:1 water) was dropped carefully on the photocatalytic surface. Irradiation (>420 nm) was carried out from the top using 300 W xenon light source (Asahi Spectra), which does not emit any IR radiation, and spectra were recorded with respect to time. All the spectra were recorded at room temperature and pressure in the range 4000–600 cm^{-1} wavenumber with a resolution of 4 cm^{-1} by averaging 32 scans. The reference spectra of 4-MBA and anisaldehyde were recorded by directly pouring the water solution on the surface of a diamond-faced ZnSe prism or ATR crystal.

3. RESULTS AND DISCUSSION

Structural details of Bi_2WO_6 or Pt/Bi_2WO_6 were investigated employing standard analytical techniques. Representative images showing the shape and morphology of sample are illustrated in Figure 1. FESEM images, Figure 1 (A and B), confirmed the formation of self-assembled spheres with hierarchical architecture. The diameter and thickness of the spheres were measured to be 2–4 μm and <1 μm, respectively. TEM images showing single sphere and its constituents (nanoplates) are presented in Figure 1 (C and D). TEM images revealed that the hierarchical structure was consisting of nanosheet-like crystallites or plates. Analysis of high resolution TEM images showed the presence of nanoporous surface, Figure 1 (E and F). The pore size was measured to be >3 nm; it corroborated the observation of BET analysis, which measured the pore size ~3.5 nm. Nitrogen adsorption–desorption isotherms and pore size distribution of various samples are given in Supporting Information Figure S5. The surface area of nonporous Bi_2WO_6, nanoporous Bi_2WO_6, Pt/nonporous Bi_2WO_6, and Pt/nanoporous Bi_2WO_6 was measured to be 24.6 m^2 g^{-1}, 34.7 m^2 g^{-1}, 37.8 m^2 g^{-1}, and 50.4 m^2 g^{-1}, respectively.

DOI: 10.1021/am507428r
ACS Appl. Mater. Interfaces 2015, 7, 1257–1269

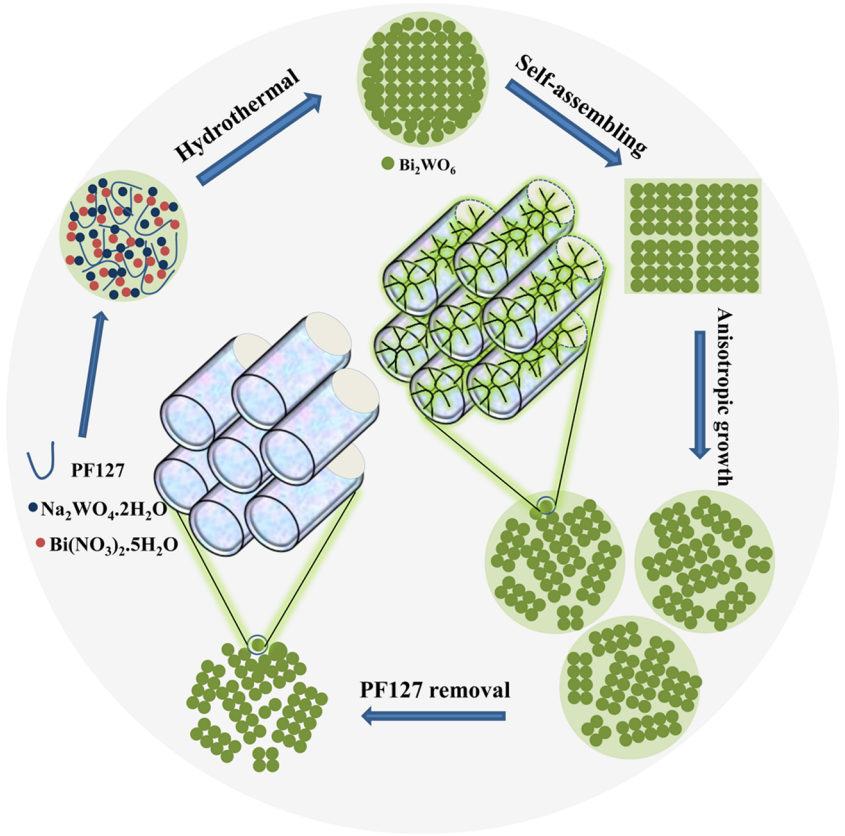

Figure 2. Schematic of plausible mechanism of nucleation, crystallization, self-assembling, and generation of porosity in nanoporous Bi_2WO_6.

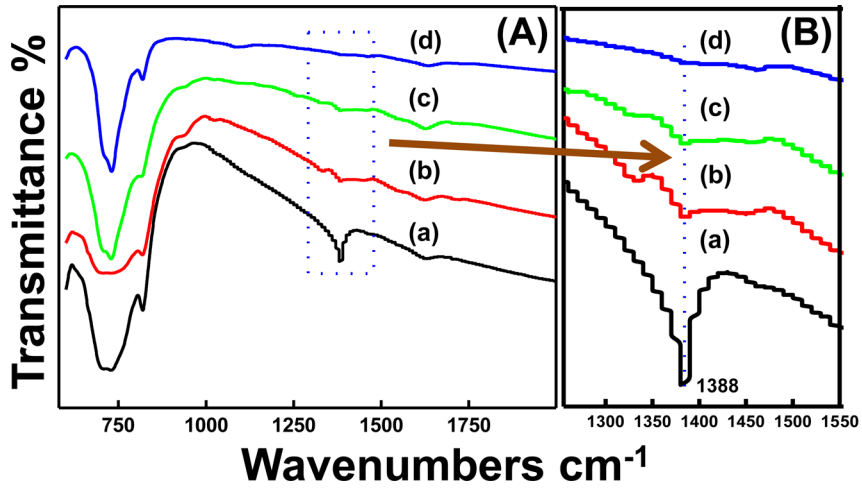

Figure 3. (A) FTIR spectra of (a) pure Bi_2WO_6, (b) 0.5%Pt/Bi_2WO_6, (c) 2%Pt/Bi_2WO_6, and (d) 5%Pt/Bi_2WO_6 and (B) magnified FTIR spectra showing preferential deposition of Pt at the adsorption site of NO_3 ions.

The shape of deposited Pt nanoparticles, Figure 1G, was observed to spherical while the size was determined to be ~2 nm. The crystalline nature of the sample was determined by XRD, Figure 1H, which confirmed a well crystalline russellite structure of bismuth tungstate.

The plausible morphological and porosity evolution of Bi_2WO_6 is schematically presented in Figure 2. Under high temperature and pressure, nucleation of bismuth tungstate is likely to take place, which may later grow into small nanoplates.

Under continuous hydrothermal heating in a highly acidic environment, these aggregated nanoparticles may further grow into a two-dimensional structure followed by crystallization, self-assembling, and anisotropic growth process, eventually leading to the formation of a crystalline flower-like hierarchical structure. Furthermore, removal of the organic surfactant generated porous surface, as illustrated in Figure 2.

Optical property of Bi_2WO_6 samples was studied by UV–visible diffuse reflectance spectroscopy. No obvious difference in absorption spectra of various samples was noticeable, and the representative absorption spectra of Pt/nonporous Bi_2WO_6 and Pt/nanoporous Bi_2WO_6 are shown in Supporting Information Figure S6. Band gap of nonporous Bi_2WO_6, Pt/nonporous Bi_2WO_6, nanoporous Bi_2WO_6, and Pt/nanoporous Bi_2WO_6 obtained by extrapolation of the plots (inserted figures) of

DOI: 10.1021/am507428r
ACS Appl. Mater. Interfaces 2015, 7, 1257–1269

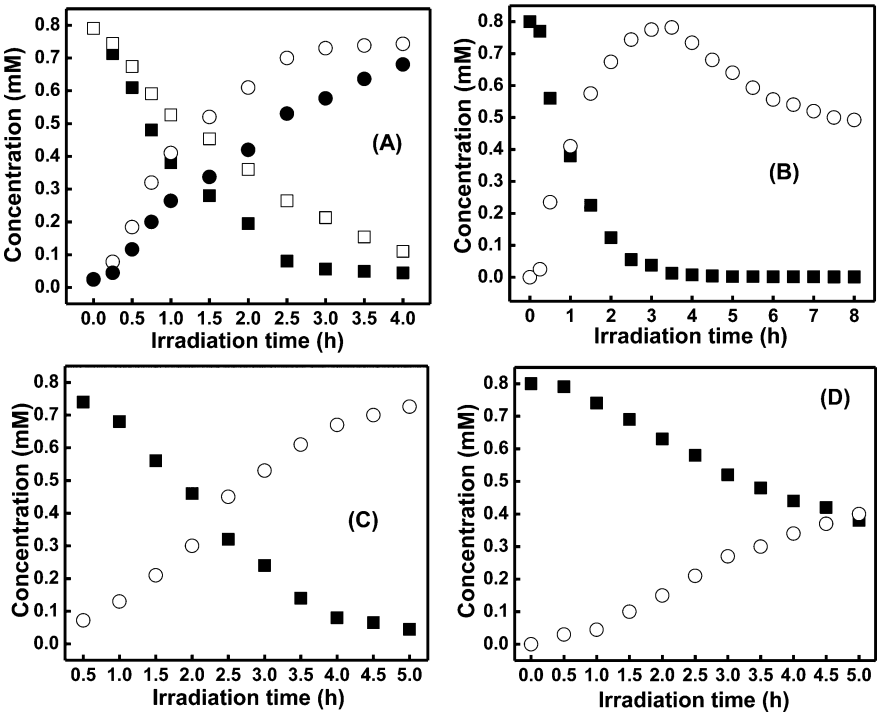

Figure 4. Change in the concentrations of alcohols and aldehydes upon irradiation: (A) 4-MBA and *p*-anisaldehyde in the presence of Pt/nanoporous Bi_2WO_6 (more active) and Pt/nonporous Bi_2WO_6 (less active), (B) 4-MBA and *p*-anisaldehyde in the presence of Pt/nanoporous Bi_2WO_6 showing the effect of longer irradiation time, (C) 4-NBA and *p*-nitrobenzaldehyde in the presence of Pt/nanoporous Bi_2WO_6, and (D) 4-MBA and *p*-anisaldehyde in the presence of nanoporous Bi_2WO_6. Experimental conditions: 4-MBA or 4-NBA concentration = 0.8 mM, 0.5%Pt/Bi_2WO_6 amount = 0.5 g L^{-1}, volume (H_2O) = 130 mL. Symbols: [■ or □] 4-MBA or 4-NBA, [● or ○] *p*-anisaldehyde or *p*-nitrobenzaldehyde.

$(ah\nu)^2$ vs $h\nu$ were 2.84 eV, 2.82 eV, 2.83 and 2.80 eV, respectively.

Pure and platinized bismuth tungstates samples were also analyzed by FTIR spectrophotometer and obtained results are shown in Figure 3. Spectra confirmed that the samples were free from any carbonaceous materials coming from surfactant. The characteristic absorption bands of Bi_2WO_6 appeared in 400−1000 cm^{-1}, which corresponded to Bi−O stretching, W−O stretching, and W−O−W bridging stretching modes. The peak at 1640 cm^{-1} could be attributed to the bending vibration of −OH group, which was seen in both pure as well as platinized samples. Moreover, symmetric stretching vibration of −OH groups of adsorbed water on Bi_2WO_6 or Pt/Bi_2WO_6 was observed at 3420 cm^{-1}. IR bands for pure as well as Pt/Bi_2WO_6 were similar, except the absorption band at 1388 cm^{-1}, which could be ascribed to the N−O vibration of nitrate ion (coming from bismuth nitrate precursor) adsorbed on Bi_2WO_6 surface.[35] Interestingly, in case of Pt/Bi_2WO_6, the intensity of this band was suppressed and disappeared as the Pt amount was increased, as shown in Figure 3B, presumably indicating that Pt clusters/nanoparticles preferentially nucleated at the adsorption site of NO_3 ions on Bi_2WO_6 surface.

Photocatalytic activity of Bi_2WO_6 synthesized at different temperature, such as 130, 150, 170, and 190 °C was investigated. Since Bi_2WO_6 synthesized at 170 °C showed the best photocatalytic activity, all the Bi_2WO_6 samples were synthesized at this temperature. All the photocatalytic reactions were carried out in water at room temperature and ambient pressure under simulated sunlight. The openings of photoreactor were properly closed in order to preclude the escape of product(s) formed during reaction. The products formed during the photooxidation of alcohols were extracted and analyzed by GC-MS analysis, in addition to ultra performance liquid chromatography (UPLC), which substantiated the GC-MS observation. A representative time-dependent variation in concentrations of 4-MBA and anisaldehyde is presented in Figure 4A.

As can be apparently seen, upon irradiation concentration of 4-MBA decreased with time and after ∼4 h of irradiation >95% of 4-MBA was converted to *p*-anisaldehyde with >95% yield and >99% selectivity. A quantitative analysis of 4-MBA and anisaldehyde concentrations revealed the mole-to-mole conversion and trace formation of any other product was not noticeable throughout the course of the reaction. Furthermore, to elucidate the effect of porosity on the photocatalytic activity, Pt/nonporous Bi_2WO_6 nanocomposite was prepared and photocatalytic activity was studied (Figure 4A). For 2.5 h irradiation time, a comparative analyses indicated a better oxidation of 4-MBA in the presence of Pt/nanoporous Bi_2WO_6 than Pt/nonporous Bi_2WO_6 under identical experimental conditions. The better efficiency of nano photocatalyst could be explained in terms of increased surface area and porosity. The high surface area and porous structure may facilitate the adsorption−desorption kinetics of 4-MBA as well as *p*-anisaldehyde formed during the photocatalytic process making the photocatalytic process more efficient. In order to follow the course of oxidation process after exhaustive alcohol oxidation, irradiation was prolonged and photocatalyst amount was increased (1.0 g L^{-1}). Figure 4B shows the change in 4-MBA concentration under prolonged irradiation, while corresponding evolution in GC-MS spectra is delineated in Supporting Information Figure S1. Interestingly, after almost complete oxidation of 4-MBA, oxidation of *p*-anisaldehyde ensued. Recently, it has been demonstrated that alcohol (methanol)

DOI: 10.1021/am507428r
ACS Appl. Mater. Interfaces 2015, 7, 1257−1269

Table 1. Comparative Oxidation of Selected Aromatic Alcohols by Heterogeneous Photocatalytic Process[a]

catalyst	substrate	product	conversion (%)	selectivity (%)	yield (%)	conditions	ref
TiO_2	BA	benzaldehyde	50	38	(*)	H_2O, UV light	14, 16
	4-MBA	*p*-anisaldehyde	50	60	(*)		
TiO_2	BA	benzaldehyde	42	95	(*)	trifluorotoluene, UV light	34
SiO_2/TiO_2	BA	benzaldehyde	46	95	(*)		
SiO_2/TiO_2 (modified with H_2SO_4)	BA	benzaldehyde	90	95	(*)		
TiO_2	4-MBA	*p*-anisaldehyde	65	(*)	41.5	H_2O, UV light	18
CdS/graphene	BA	benzaldehyde	45	90	45	trifluorotoluene, visible light	12
CdS/graphene/TiO_2	BA	benzaldehyde	>80	>90	<80	trifluorotoluene, visible light	13
Au/CeO_2	BA	benzaldehyde	>99	>99	>99	H_2O, visible light	23, 24
TiO_2	4-MBA	*p*-anisaldehyde	50	56	(*)	H_2O, UV light	19
Pt/TiO_2	BA	benzaldehyde	87	68	(*)	H_2O, visible light	21
	4-MBA	*p*-anisaldehyde	85	90	(*)		
	Cinnamyl alcohol	cinnamaldehyde	95	71	(*)		
Ir/TiO_2	BA	benzaldehyde	~9	92	(*)	H_2O, UV light	22
WO_3/TiO_2	BA	benzaldehyde	50	56	(*)	H_2O, light >350 nm	36
HNb_3O_8	BA	benzaldehyde	20	>99	(*)	benzotrifluoride, visible light	47
	4-MBA	*p*-anisaldehyde	63	85	(*)		
Ag_3PO_4	BA	benzaldehyde	>85	>99	~85	H_2O, simulated sunlight	48
	4-MBA	*p*-anisaldehyde	>85	>99	~85		
	Cinnamyl alcohol	cinnamaldehyde	~90	>90	~81		
Pt/Bi_2WO_6	4-MBA	*p*-anisaldehyde	>95	>99	~95	H_2O, simulated sunlight	this study
	4-NBA	*p*-nitrobenzaldehyde	>85	>99	~85		

[a](*) not mentioned; BA, benzyl alcohol; 4-MBA, 4-methoxy benzyl alcohol.

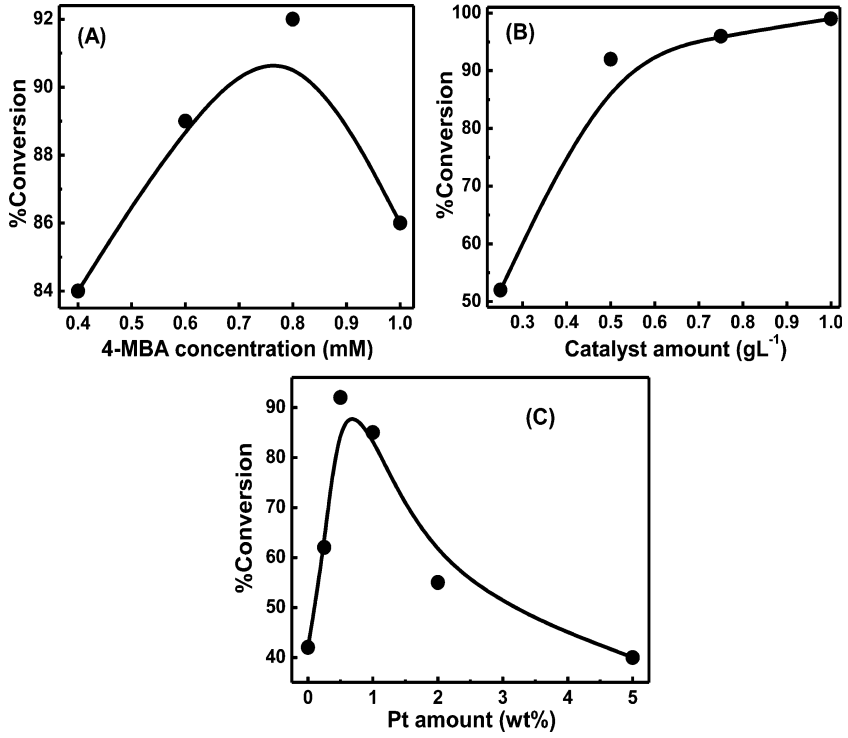

Figure 5. Dependence of 4-MBA oxidation on (A) 4-MBA concentration, (B) Pt/nanoporous Bi_2WO_6 amount, and (C) Pt amount deposited on nanoporous Bi_2WO_6. Experimental conditions: irradiation time = 4 h, 4-MBA concentration = 0.8 mM, 0.5%Pt/Bi_2WO_6 amount = 0.5 g L^{-1}, volume (H_2O) = 130 mL.

could also be completely oxidized only into CO_2 and H_2, the formation of any other gaseous or liquid products was not observed.[36] In addition to 4-MBA, conversion of 4-nitrobenzyl alcohol (4NBA) was also studied to evaluate and verify the selectivity and efficiency of Pt/nanoporous Bi_2WO_6 toward other alcohol. Furthermore, selection of 4-NBA would also

DOI: 10.1021/am507428r
ACS Appl. Mater. Interfaces 2015, 7, 1257−1269

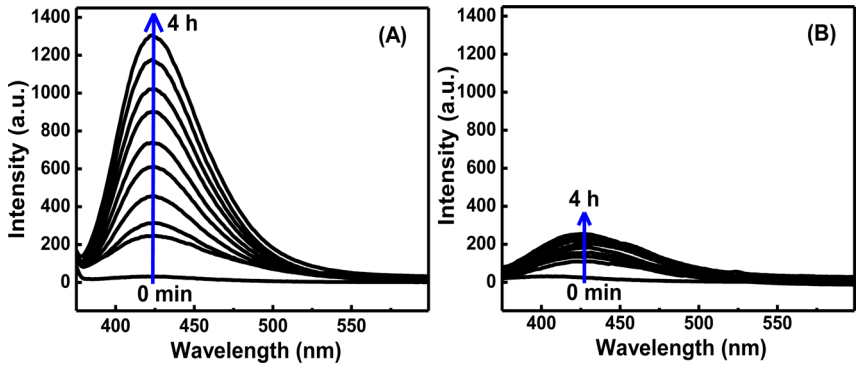

Figure 6. Change in fluorescence intensity of terephthalic acid as a function of irradiation time in aqueous suspensions of Pt/nanoporous Bi_2WO_6: (A) in absence and (B) presence of 4-MBA.

shed light on the effect of the electron withdrawing substituent on the oxidation process. Results are presented in Figure 4C, which showed that 4-NBA underwent >85% oxidation forming 4-nitrobenzaldehyde with >85% yield and selectivity exceeding 99% (on mole-to-mole conversion basis), though 4-NBA oxidized slower than that of 4-MBA. A slower oxidation of 4-NBA could be ascribed to the electron withdrawing attributes of nitro group, which makes $-CH_2-OH$ electron deficient and thus somewhat resistant to oxidation. Moreover, oxidation of some selected aliphatic alcohols, namely 1-butanol, 1-pentanol, and 1-hexanol, was also investigated in the presence of Pt/nanoporous Bi_2WO_6 under identical conditions, and the results are presented in Supporting Information Figure S2. As could be seen, the conversion of aliphatic alcohols was slow (~25%) after 4 h of irradiation. Although the major product was the corresponding aldehydes, trace formation of other byproducts was also observed. Furthermore, the oxidation of 4-MBA was also examined in the presence of pure Bi_2WO_6, and the results, presented in Figure 4D, indicated <45% conversion, though the selectivity was maintained.

Unlike previous reports, as presented in Table 1, in which one of the predominant constraints in achieving selective oxidation by photocatalytic process has been the overoxidation of reactants or products during longer irradiation time, this study presents a peculiar example of a complete oxidation of alcohol followed by aldehyde in the presence of Pt/Bi_2WO_6. In a recent study,[37] the overoxidation was correlated with the complexation of aldehydes, unlike alcohol, which does not complex, with TiO_2 surface. When TiO_2 surface was substantially covered with the layers of WO_3, overoxidation was much averted because WO_3 was found to be inactive for aldehyde oxidation. In this study, to investigate if there is any interaction between *p*-anisaldehyde and Pt/Bi_2WO_6 surface, adsorption experiments were carried out and any change in catalyst's surface was followed by FTIR while any change in aldehyde concentration was analyzed by GC-MS. FTIR spectra, presented Supporting Information Figure S7, showed identical patterns and the presence of any trace of aldehyde was not noticeable. Furthermore, GC-MS analysis did not indicate any decrease in aldehyde concentrations. The dearth of noticeable physisorption of *p*-anisaldehyde onto the surface of Pt/Bi_2WO_6 explains, to a certain extent, the suppression of aldehyde oxidation.

From a mechanistic and application standpoint, it is important to correlate the dependence of oxidation with the substrate concentration, the catalyst loading, and the amount of deposited Pt.

Therefore, the effect of such parameters was investigated, and the results are illustrated in Figure 5. As readily seen, the oxidation increased monotonically with 4-MBA concentration up to 0.8 mM followed by a decrease at higher concentration. This could be due to the fact that up to 0.8 mM 4-MBA concentration, sufficient number of active sites is available on the photocatalyst's surface, which promote oxidation and hence lead to higher conversion. Decrease in percent conversion at 1.0 mM could be attributed to the existence of a finite number of active sites. Since the highest conversion was observed at 0.8 mM concentration of 4-MBA, the effect of catalyst loading on percentage conversion was investigated at this optimal 4-MBA concentration.

The obtained conversion trend showed a parabolic dependence, which is a characteristic of heterogeneous catalytic process. Besides the availability of more photocatalyst's surface, an increase in the amount of photocatalyst leads to more photon absorption, which in turn generates a higher amount of active surface or photoexcited holes in the valence band for oxidation. This triggers interfacial electron transfer from 4-MBA to the valence band holes, causing an increase in conversion. Since Pt nanoparticles deposited onto the surface of Bi_2WO_6 significantly improved the photocatalytic activity, the amount of deposited Pt may play an important role in the optimization of the photocatalytic oxidation of 4-MBA. Change in alcohol and aldehyde concentrations or % conversion with respect to Pt amounts (0.25, 0.5, 1.0, 2.0, and 5.0 wt %) is presented in Figure 5C. As could be apparently seen, the highest conversion was obtained with 0.5 wt % Pt, followed by a decrease at higher Pt loadings. The improvement in oxidation in the presence of platinized bismuth tungstate may be attributed to the possible formation of a Schottky barrier between Pt and Bi_2WO_6. In general, the formation of a Schottky barrier between noble metals and semiconductor photocatalysts has been discussed previously by other authors.[4,38,39] At higher Pt loadings, decrease in the oxidation efficiency may be rationalized in terms of the fact that substantial coverage of photocatalyst's surface by Pt may take place, which could potentially serve as a shield and prevent the incident photons from impinging on the Bi_2WO_6 surface, thereby decreasing the photocatalytic performance.[40] Under the optimized experimental conditions, the reaction rate for the conversion of alcohol was calculated to be 0.2 mM h^{-1}, using 1 g L^{-1} photocatalyst amount, which is to the best of our knowledge the highest rate reported as yet under photocatalytic conditions.

DOI: 10.1021/am507428r
ACS Appl. Mater. Interfaces 2015, 7, 1257−1269

In most of the earlier documented studies relating to the photocatalytic oxidation, the selectivity was essentially maintained up to a certain degree of alcohol oxidation (ca. 60%) and the selectivity diminished as the reaction proceeded owing to the overoxidation of byproducts, oxidation of the aldehyde for instance. Interestingly, the selectivity toward *p*-anisaldehyde sustained with Pt/Bi_2WO_6 until exhaustive oxidation of 4-MBA took place, followed by further oxidation of *p*-anisaldehyde. Substantially, the nonselective behavior of semiconductor-mediated photocatalytic process could be attributed to the formation of extremely reactive and short-lived radicals such as $OH^{\bullet}$, $O_2^{-\bullet}$, $HO_2^{\bullet}$, etc. The mechanism for the formation of such radicals has been extensively discussed in the literature by a multitude of authors. Briefly, an exciton (e^- and h^+ pair) could be generated in photocatalysts upon providing appropriate photonic energy (equal to or greater than the band gap). Excited conduction band electrons could readily reduce O_2 to $O_2^{-\bullet}$ while the holes in the valence band can oxidize water, generating $OH^{\bullet}$ radicals. As stated above, these radical species are very reactive, though short-lived, and make the photocatalytic process nonselective. Hence, in order to determine and interpret the operative mechanism responsible for the high selectivity, the involvement of such radicals in the oxidation process was examined.

Since terephthalic acid is an excellent trapping agent for $OH^{\bullet}$, gets transformed into fluorescent 2-hydroxyterephthalic,[41] it was utilized as a probe molecule to monitor the formation of $OH^{\bullet}$ in the reaction media. The change in fluorescence intensity, which is a function of OH radicals, was monitored by photoluminescence. Formation of $OH^{\bullet}$ in the reaction media was followed both in the absence and presence of 4-MBA, and the results are illustrated in Figure 6. A significant amount of 2-hydroxyterephthalic was formed with respect to irradiation time, as indicated by the high intensity, when terephthalic acid was irradiated without 4-MBA, suggesting the generation of $OH^{\bullet}$ via oxidation of H_2O. However, when irradiation was performed in the presence of 4-MBA, the PL intensity was significantly attenuated revealing the predominant oxidation of alcohol over that of water. This suggested that the involvement of OH radicals in the oxidation of alcohol is less likely.

There appears to be a discrepancy in the literature about the generation of OH radical through Bi_2WO_6. For instance, Zhu et al. studied the degradation and mineralization of bisphenol A by Bi_2WO_6 and did not find any hydroxylated product formed during the photocatalytic process.[42] The absence of any hydroxylated product was explained in terms of standard oxidation potential of photogenerated hole (1.59 eV), which is lower than the redox potential of $HO^{\bullet}/OH^-$ (1.99 eV). However, some recent investigations clearly presented the evidence for the formation of OH radicals through the water oxidation by valence band holes of Bi_2WO_6.[33,43,44] Our results seem to essentially support the earlier findings that OH radical could be generated through water oxidation on the surface of Bi_2WO_6.

Relatively, the involvement of O_2 is intricate as compared to OH radicals because O_2 can play a dual role: it could either be directly incorporated to yield oxygenated product or serve as the conduction band electron acceptor, in the photocatalytic oxidation process.[11] In order to elucidate the rate determining factor and to shed light on the operative mechanism, oxidation of alcohol was studied in the presence of various radical and electron scavenging entities, such as molecular O_2 and N_2, hydroquinone, ammonium persulfate ($(NH_4)_2S_2O_8$), and ammonium oxalate ($(NH_4)_2C_2O_4$), and obtained results are illustrated in Figure 7. To determine the role of O_2, the

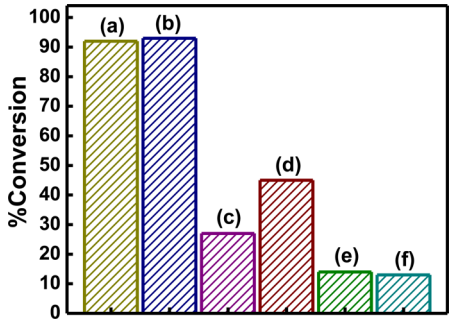

Figure 7. Effect of electron, hole, and $O_2^{-\bullet}$ radical scavengers on the photocatalytic oxidation of 4-MBA: (a) under dissolved oxygen, (b) under bubbling of O_2, (c) in the absence of O_2 or under bubbling of N_2, (d) in the absence of O_2 or presence of $(NH_4)_2S_2O_8$, (e) in the presence of hydroquinone, and (f) in the presence of $(NH_4)_2C_2O_4$. Experimental condition: irradiation time = 4 h, 4-MBA concentration = 0.8 mM, 0.5%Pt/nanoporous Bi_2WO_6 amount = 0.5 g L^{-1}, volume (H_2O) = 130 mL.

oxidation of 4-MBA was carried out both in the absence and presence of molecular O_2, by bubbling N_2 or O_2 through photoreactor. Results, presented in Figure 7, showed that the conversion was profoundly dependent on the ambient environment. Apparently, the oxidation in the absence of oxygen was slow (ca. 27%), indicating that O_2 played significant role in the oxidation of 4-MBA. Oxidation was also assessed under highly O_2-saturated environment, O_2 was bubbled throughout the course of the reaction, but inconsequential improvement was observed and obtained results were analogous to that of obtained only with dissolved oxygen. This indicated that the dissolved O_2 is adequate to drive the effective oxidation and the process was independent of any oxygen transport limitation. To further delve into the O_2 involvement, reactions were carried out employing $(NH_4)_2S_2O_8$ as an alternative electron acceptor in the absence of O_2 where ~45% conversion was noticed. This observation indicated that O_2 is serving as an effective electron acceptor, which attenuates the recombination of exciton, during the oxidation of 4-MBA. Moreover, hydroquinone and $(NH_4)_2C_2O_4$ were employed as a hole trap, and the extent of oxidation was investigated. As presented in Figure 7, the oxidation of 4-MBA was found to be only ~12% in the presence of these hole scavengers. Interestingly, the results obtained in the presence of $(NH_4)_2C_2O_4$ were comparable to that obtained in the presence of hydroquinone. This observation apparently revealed the critical involvement of valence band holes, rather than O_2, in the oxidation. Based on such findings, a plausible mechanism involving various possible pathways is presented in Scheme 1.

However, it seems rational to postulate that the two-step oxidation of 4-MBA predominantly took place through valence band holes, which also appears to be a rate-determining step, while O_2 primarily contributed in the improvement of photocatalytic efficiency by preventing electron−hole pair recombination. Moreover, path B seems more likely as the formation of radical at the *β*-carbon may result in the delocalization of this electron in the adjacent benzene ring,

DOI: 10.1021/am507428r
ACS Appl. Mater. Interfaces 2015, 7, 1257−1269

Scheme 1. Probable Mechanism of 4-MBA Oxidation in the Presence of Pt/Bi_2WO_6 under Light

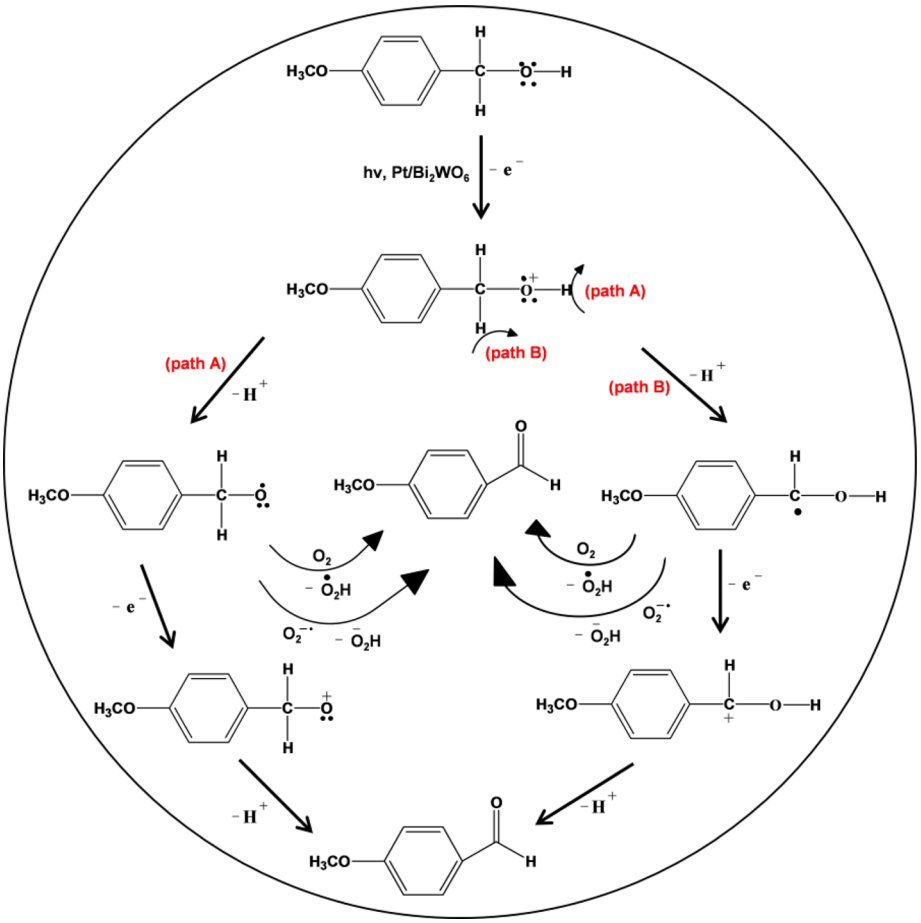

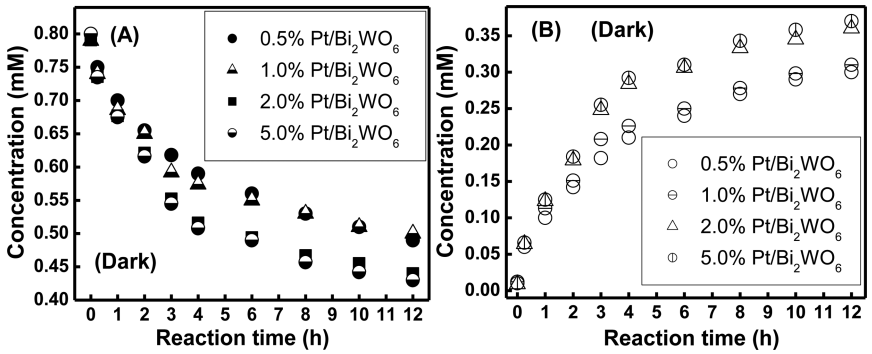

Figure 8. (A) Change in 4-MBA concentration and (B) formation of *p*-anisaldehyde under dark in the presence of nanoporous Bi_2WO_6 having various amounts of Pt. Experimental conditions: 4-MBA concentration = 0.8 mM, photocatalyst amount = 1.0 g L^{-1}, volume (H_2O) = 130 mL.

imparting additional stability and rather thermodynamically favorable oxidation.

With the noted fact that noble metal supported catalysts are capable of driving oxidation of alcohols, oxidation of 4-MBA was investigated under dark in aqueous suspensions of Pt/Bi_2WO_6. Decrease in alcohol concentration and formation of aldehyde, as a function of Pt amounts (0.5, 1.0, 2.0, and 5.0 wt %), deposited on nanoporous Bi_2WO_6 are shown in Figure 8. It could be readily seen that the noticeable formation of aldehyde took place even in the dark. However, change in 4-MBA concentration or the formation of *p*-anisaldehyde was not noticeable in the presence of pure Bi_2WO_6. Oxidation of alcohols on the surface of the noble metals, supported or unsupported, has been discussed previously,[45,46] and critical steps involved are presented in Scheme 2. Briefly, the reaction starts by the adsorption of alcohols onto the catalyst's surface followed by the formation of metal alkoxide and metal hydride (on the neighboring Pt atom). The adsorbed metal alkoxide undergoes *β*-hydride elimination process producing aldehyde, though ketones may also be produced at this stage but were not observed in this study. Finally, the adsorbed hydrogen undergoes oxidation through molecular oxygen producing water molecule and regenerating the Pt active sites for the further oxidation.

The course of oxidation reaction was also followed by an in situ ATR-FTIR analysis, and the study was performed in

DOI: 10.1021/am507428r
ACS Appl. Mater. Interfaces 2015, 7, 1257−1269

Scheme 2. Probable Mechanism of 4-MBA Oxidation in the Presence of Pt/Nanoporous Bi_2WO_6 under Dark

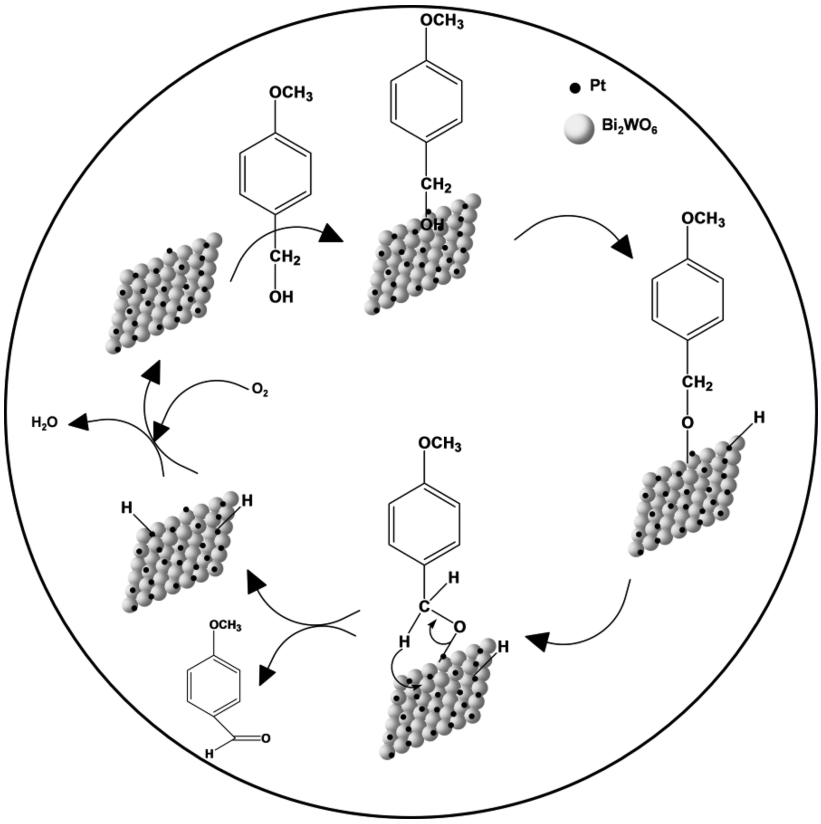

conditions analogous to photocatalytic conditions. A time-dependent evolution in ATR-FTIR spectra in the presence of both pure and Pt/Bi_2WO_6 under light and darkness is presented in Figure 9. The spectra of 4-MBA and anisaldehyde solution prepared in water have also been included in Figure 9 for comparison.

In the case of Pt/Bi_2WO_6, both under light and darkness, the intensity of some of the bands was decreased while the intensity of some bands was increased. Absorption bands of 4-MBA evolved gradually with time and started to resemble to that of anisaldehyde. Notably, the absorption band corresponding to the C═O stretching vibration, which essentially differentiate 4-MBA and anisaldehyde, apparently appeared at ∼1678 cm^{-1}. Under light, this band appeared after 10 min of irradiation and the intensity was steadily increased with irradiation time, whereas, under dark, it became apparent after 150 min and the intensity continued to grow as a function of time. In situ investigation was also carried out in the presence of Bi_2WO_6 modified with 2 wt % Pt under dark, no noticeable difference was observed as compared to that of 0.5 wt % Pt except the C═O stretching vibration at ∼1678 cm^{-1} was more intense in the case of 2 wt % Pt/Bi_2WO_6. Parts C and D of Figure 9 show the change in 4-MBA spectra, under light and dark respectively, in the presence of pure Bi_2WO_6. As could be seen, the distinctive band at ∼1678 cm^{-1} was detected after prolong irradiation (90 min), and the intensity was observed to be much less as compared to that of Pt/Bi_2WO_6. Furthermore, this band was absent in the presence of pure Bi_2WO_6 under dark, which essentially substantiated the earlier observation that Pt/Bi_2WO_6 is efficacious in oxidizing 4-MBA under dark.

To investigate the stability and the recyclability of Pt/Bi_2WO_6, experiments were carried out under the identical conditions, as described in the photocatalytic experiments section. After the completion of each run, the catalyst was collected, washed, dried (300 °C), and utilized for the next runs under the identical conditions. The photocatalytic formation of *p*-anisaldehyde from 4-MBA as a function of different runs is illustrated in Figure 10. As could be seen, Pt/Bi_2WO_6 is an efficient, recyclable photocatalyst for the selective oxidation of 4-MBA. Furthermore, the XRD patterns recorded after several runs did not indicate any change in crystal structure of Pt/Bi_2WO_6 demonstrating the chemical stability of the photocatalyst under applied experimental conditions.

4. CONCLUSIONS

In summary, highly efficient, selective, and quantitative conversion of aromatic alcohols into their corresponding aldehydes (mole-to-mole conversion) could be achieved in the presence of nanoporous hierarchical Pt/Bi_2WO_6 spheres in water under mild conditions under simulated sunlight. High efficiency of Bi_2WO_6 could be attributed to nanoporous surface and hierarchical architecture, besides Pt nanoparticles that prevented the recombination of exciton. Alcohol competed with water and predominantly oxidized minimizing the generation of $OH^{\bullet}$ resulting from water splitting. Based on this, it appears rational to envisage that the reduction site of the semiconductor photocatalysts is more pivotal to be engineered in order to obtain high selective oxidation of alcohols. Furthermore, it is postulated that the valence band holes are the primary catalytic sites for the two-step oxidation of alcohols, rather than direct oxidation through molecular oxygen, under studied photocatalytic conditions. Nanocomposite Pt/Bi_2WO_6 showed a considerable conversion of 4-MBA into *p*-anisaldehyde under dark, though the conversion was relatively

DOI: 10.1021/am507428r
ACS Appl. Mater. Interfaces 2015, 7, 1257−1269

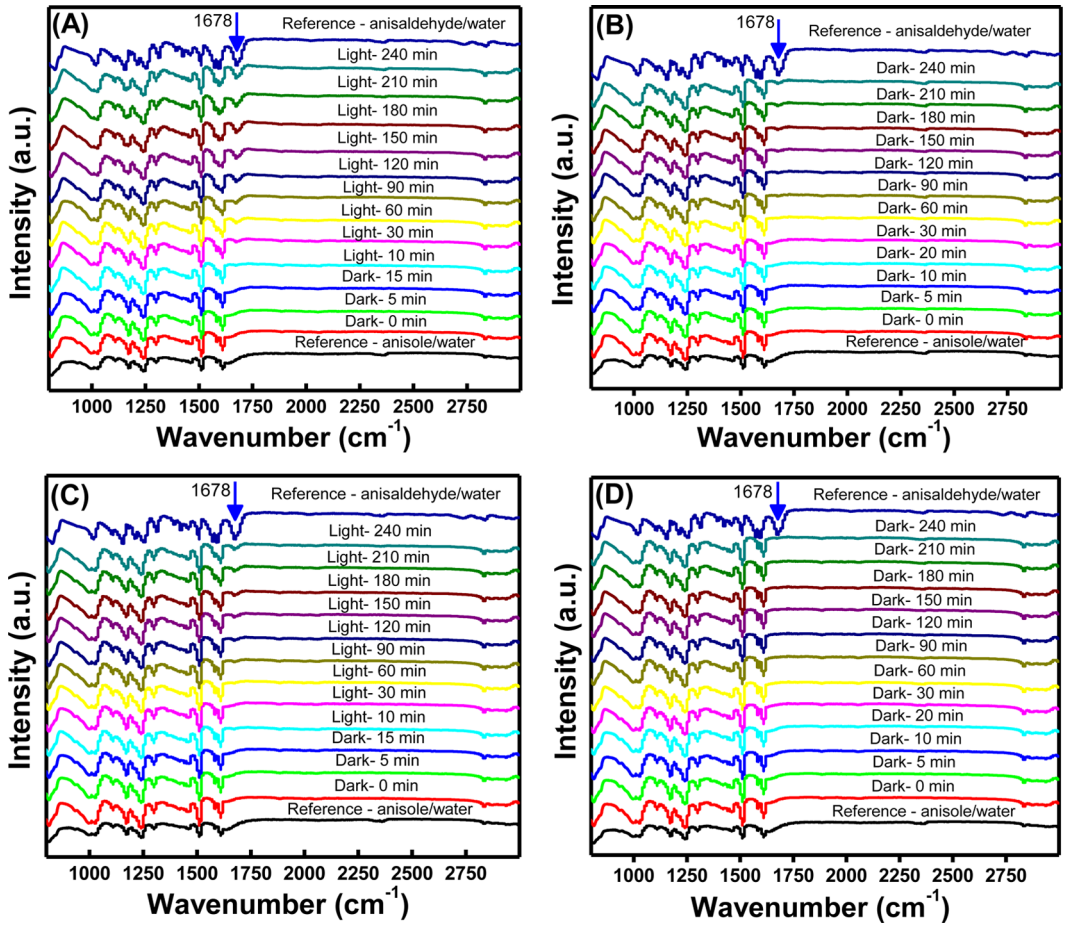

Figure 9. Change in selected ATR-FTIR spectra of 4-MBA in the presence of Pt/nanoporous Bi_2WO_6 (A) under light and (B) under dark, and in the presence of pure nanoporous Bi_2WO_6 (C) under light and (D) under dark.

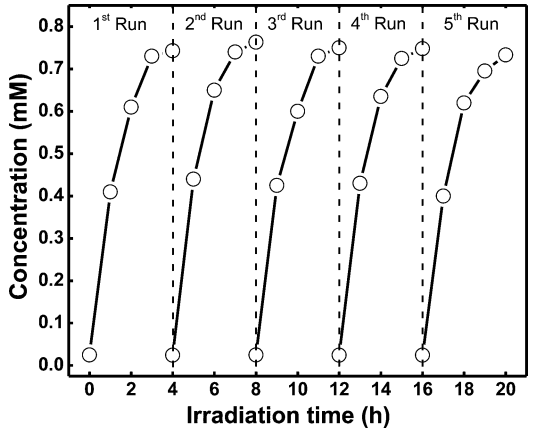

Figure 10. Effect of recycling on the photocatalytic performance of Pt/nanoporous Bi_2WO_6 for the conversion of 4-MBA into *p*-anisaldehyde.

slow. Furthermore, the photocatalyst was chemically stable and showed efficient recyclability.

■ ASSOCIATED CONTENT

Supporting Information

GC-MS spectra showing the time-dependent conversion of 4-MBA into *p*-anisaldehyde, oxidation of aliphatic alcohols, Raman spectrum, EDS spectrum, N_2 adsorption−desorption isotherms, UV−visible diffuse reflectance spectra, FTIR spectra, and schematic of the photoreactor. This material is available free of charge via the Internet at http://pubs.acs.org.

■ AUTHOR INFORMATION

Corresponding Authors

*E-mail: qamar@kfupm.edu.sa.

*E-mail: bahnemann@iftc.uni-hannover.de.

Author Contributions

The manuscript was written through the contributions of all authors. All authors have given approval to the final version of the manuscript.

Notes

The authors declare no competing financial interest.

■ ACKNOWLEDGMENTS

The authors acknowledge the support provided by King Abdulaziz City for Science and Technology (KACST) through the Science and Technology Unit at King Fahd University of Petroleum and Minerals (KFUPM) for funding this work through project No. 10-NAN1387-04 as part of the National Science, Technology, and Innovation Plan. The support of the Center of Excellence in Nanotechnology and Department of Chemistry, KFUPM is gratefully acknowledged.

■ REFERENCES

(1) Miyamura, H.; Matsubara, R.; Miyazaki, Y.; Kobayashi, S. Aerobic Oxidation of Alcohols at Room Temperature and Atmospheric

DOI: 10.1021/am507428r
ACS Appl. Mater. Interfaces 2015, 7, 1257−1269

Conditions Catalyzed by Reusable Gold Nanoclusters Stabilized by the Benzene Rings of Polystyrene Derivatives. *Angew. Chem., Int. Ed.* **2007**, *119*, 4229−4232.
(2) Hundlucky, M. *Oxidations in Organic Chemistry*; American Chemical Society: Washington, DC, 1990.
(3) Uozumi, Y.; Nakao, R. Catalytic Oxidation of Alcohols in Water under Atmospheric Oxygen by Use of an Amphiphilic Resin-Dispersion of a Nanopalladium Catalyst. *Angew. Chem., Int. Ed.* **2003**, *42*, 194−197.
(4) Hoffmann, M. R.; Martin, S. T.; Choi, W.; Bahnemann, D. W. Environmental Applications of Semiconductor Photocatalysis. *Chem. Rev.* **1995**, *95*, 69−96.
(5) Turchi, C. S.; Ollis, D. F. Photocatalytic Degradation of Organic Water Contaminants: Mechanisms Involving Hydroxyl Radical Attack. *J. Catal.* **1990**, *122*, 178−192.
(6) Kamat, P. V. Meeting the Clean Energy Demand: Nanostructure Architectures for Solar Energy Conversion. *J. Phys. Chem. C* **2007**, *111*, 2834−2860.
(7) Maeda, K.; Teramura, K.; Lu, D.; Takata, T.; Saito, N.; Inoue, Y.; Domen, K. Photocatalyst Releasing Hydrogen from Water. *Nature* **2006**, *440*, 295−295.
(8) Varghese, O. K.; Paulose, M.; LaTempa, T. J.; Grimes, C. A. High-Rate Solar Photocatalytic Conversion of CO_2 and Water Vapor to Hydrocarbon Fuels. *Nano Lett.* **2009**, *9*, 731−737.
(9) Yoon, T. P.; Ischay, M. A.; Du, J. Visible Light Photocatalysis as a Greener Approach to Photochemical Synthesis. *Nat. Chem.* **2010**, *2*, 527−532.
(10) Palmisano, G.; Augugliaro, V.; Pagliaro, M.; Palmisano, L. Photocatalysis: A Promising Route for 21st Century Organic Chemistry. *Chem. Commun.* **2007**, 3425−3437.
(11) Lang, X.; Chen, X.; Zhao, J. Heterogeneous Visible Light Photocatalysis for Selective Organic Transformations. *Chem. Soc. Rev.* **2014**, *43*, 473−486.
(12) Zhang, N.; Zhang, Y. P. X.; Fu, X.; Liu, S.; Xu, Y.-J. Assembly of CdS Nanoparticles on the Two-Dimensional Graphene Scaffold as Visible-Light-Driven Photocatalyst for Selective Organic Transformation under Ambient Conditions. *J. Phys. Chem. C* **2011**, *115*, 23501−23511.
(13) Zhang, N.; Zhang, Y.; Pan, X.; Yang, M.-Q.; Xu, Y.-J. Constructing Ternary CdS−Graphene−TiO_2 Hybrids on the Flatland of Graphene Oxide with Enhanced Visible-Light Photoactivity for Selective Transformation. *J. Phys. Chem. C* **2012**, *116*, 18023−18031.
(14) Yurdakal, D.; Palmisano, G.; Loddo, V.; Augugliaro, V.; Palmisano, L. Nanostructured Rutile TiO_2 for Selective Photocatalytic Oxidation of Aromatic Alcohols to Aldehydes in Water. *J. Am. Chem. Soc.* **2008**, *130*, 1568−1569.
(15) Maldotti, A.; Molinari, A.; Amadelli, R. Photocatalysis with Organized Systems for the Oxofunctionalization of Hydrocarbons by O_2. *Chem. Rev.* **2002**, *102*, 3811−3836.
(16) Palmisano, G.; Garcia-Lopez, E.; Marci, G.; Loddo, V.; Yurdakal, S.; Augugliaro, V.; Palmisano, L. Advances in Selective Conversions by Heterogeneous Photocatalysis. *Chem. Commun.* **2010**, *46*, 7074−7089.
(17) Augugliaro, V.; Caronna, T.; Loddo, V.; Marc, G.; Palmisano, G.; Palmisano, L.; Yurdakal, S. Oxidation of Aromatic Alcohols in Irradiated Aqueous Suspensions of Commercial and Home-Prepared Rutile TiO_2: A Selectivity Study. *Chem.—Eur. J.* **2008**, *14*, 4640−4646.
(18) Palmisano, G.; Yurdakal, S.; Augugliaro, V.; Loddo, V.; Palmisano, L. Photocatalytic Selective Oxidation of 4-Methoxybenzyl Alcohol to Aldehyde in Aqueous Suspension of Home-Prepared Titanium Dioxide Catalyst. *Adv. Synth. Catal.* **2007**, *349*, 964−970.
(19) Addamo, M.; Augugliaro, V.; Bellardita, M.; Paola, A. D.; Loddo, V.; Palmisano, G.; Palmisano, L.; Yurdakal, S. Environmentally Friendly Photocatalytic Oxidation of Aromatic Alcohol to Aldehyde in Aqueous Suspension of Brookite TiO_2. *Catal. Lett.* **2008**, *126*, 58−62.
(20) Furukawa, S.; Shishido, T.; Teramura, K.; Tanaka, T. Photocatalytic Oxidation of Alcohols over TiO_2 Covered with Nb_2O_5. *ACS Catal.* **2012**, *2*, 175−179.
(21) Zhai, W.; Xue, S.; Zhu, A.; Luo, Y.; Tian, Y. Plasmon-Driven Selective Oxidation of Aromatic Alcohols to Aldehydes in Water with Recyclable Pt/TiO_2 Nanocomposites. *ChemCatChem* **2011**, *3*, 127−130.
(22) Feng, W.; Wu, G.; Li, L.; Guan, N. Solvent-Free Selective Photocatalytic Oxidation of Benzyl Alcohol over Modified TiO_2. *Green Chem.* **2011**, *13*, 3265−3272.
(23) Tanaka, A.; Hashimoto, K.; Kominami, H. Selective Photocatalytic Oxidation of Aromatic Alcohols to Aldehydes in an Aqueous Suspension of Gold Nanoparticles Supported on Cerium(IV) Oxide under Irradiation of Green Light. *Chem. Commun.* **2011**, *47*, 10446−10448.
(24) Tanaka, A.; Hashimoto, K.; Kominami, H. Preparation of Au/CeO_2 Exhibiting Strong Surface Plasmon Resonance Effective for Selective or Chemoselective Oxidation of Alcohols to Aldehydes or Ketones in Aqueous Suspensions under Irradiation by Green Light. *J. Am. Chem. Soc.* **2012**, *134*, 14526−14533.
(25) Ma, D.; Huang, S.; Chen, W.; Hu, S.; Shi, F.; Fan, K. Self-Assembled Three-Dimensional Hierarchical Umbilicate Bi_2WO_6 Microspheres from Nanoplates: Controlled Synthesis, Photocatalytic Activities, and Wettability. *J. Phys. Chem. C* **2009**, *113*, 4369−4374.
(26) Zhang, L.; Zhu, Y. A Review of Controllable Synthesis and Enhancement of Performances of Bismuth Tungstate Visible-Light-Driven Photocatalysts. *Catal. Sci. Technol.* **2012**, *2*, 694−706.
(27) Zhang, C.; Zhu, Y. F. Synthesis of Square Bi_2WO_6 Nanoplates as High-Activity Visible-Light-Driven Photocatalysts. *Chem. Mater.* **2005**, *17*, 3537−45.
(28) Amano, F.; Yamakata, A.; Nogami, K.; Osawa, M.; Ohtani, B. Visible Light Responsive Pristine Metal Oxide Photocatalyst: Enhancement of Activity by Crystallization under Hydrothermal Treatment. *J. Am. Chem. Soc.* **2008**, *130*, 17650−17651.
(29) Ng, C.; Iwase, A.; Ng, Y. H.; Amal, R. Transforming Anodized WO_3 Films into Visible-Light-Active Bi_2WO_6 Photoelectrodes by Hydrothermal Treatment. *J. Phys. Chem. Lett.* **2012**, *3*, 913−918.
(30) Guo, Y.; Zhang, G.; Liu, J.; Zhang, Y. Hierarchically Structured a-Fe_2O_3/Bi_2WO_6 Composite for Photocatalytic Degradation of Organic Contaminants under Visible Light Irradiation. *RSC Adv.* **2013**, *3*, 2963−2970.
(31) Zhang, L. W.; Wang, Y. J.; Cheng, H. Y.; Yao, W. Q.; Zhu, Y. F. Synthesis of Porous Bi_2WO_6 Thin Films as Efficient Visible-Light-Active Photocatalysts. *Adv. Mater.* **2009**, *21*, 1286−1290.
(32) Fu, H.; Pan, C.; Yao, W.; Zhu, Y. Visible-Light-Induced Degradation of Rhodamine B by Nanosized Bi_2WO_6. *J. Phys. Chem. B* **2005**, *109*, 22432−22439.
(33) Zhang, Y.; Zhang, N.; Tang, Z.-R.; Xue, Y.-J. Identification of Bi_2WO_6 as a Highly Selective Visible-Light Photocatalyst Toward Oxidation of Glycerol to Dihydroxyacetone in Water. *Chem. Sci.* **2013**, *4*, 1820−1824.
(34) Xiong, J. Y. J.; Chen, B.; Yu, Y.; Wang, J. Hydrothermal Preparation and Visible-Light Photocatalytic Activity of Bi_2WO_6 Powders. *J. Sol. Stat. Chem.* **2005**, *178*, 1968−1972.
(35) Kandiel, T. A.; Ivanovab, I.; Bahnemann, D. W. Long-Term Investigation of the Photocatalytic Hydrogen Production on Platinized TiO_2: An Isotopic Study. *Energy Environ. Sci.* **2014**, *7*, 1420−1425.
(36) Tsukamoto, D.; Ikeda, M.; Shiraishi, Y.; Hara, T.; Ichikuni, N.; Tanaka, S.; Hirai, T. Selective Photocatalytic Oxidation of Alcohols to Aldehydes in Water by TiO_2 Partially Coated with WO_3. *Chem.—Eur. J.* **2011**, *17*, 9816−9824.
(37) Siemon, U.; Bahnemann, D.; Testa, J. J.; Rodriguez, D.; Litter, M. I.; Bruno, N. Heterogeneous Photocatalytic Reactions Comparing TiO_2 and Pt/TiO_2. *J. Photochem. Photobiol., A* **2002**, *148*, 247−255.
(38) Warner, R. M.; Grung, B. L. *Transistors: Fundamentals for the Integrated-Circuit Engineer*; John Wiley & Sons: New York, 1983.
(39) Sun, B.; Vorontsov, A. V.; Smirniotis, P. G. Role of Platinum Deposited on TiO_2 in Phenol Photocatalytic Oxidation. *Langmuir* **2003**, *19*, 3151−3156.
(40) Ishibashi, K.; Fujishima, A.; Watanabe, T.; Hashimoto, K. Detection of Active Oxidative Species in TiO_2 Photocatalysis Using the Fluorescence Technique. *Electrochem. Commun.* **2000**, *2*, 207−210.

DOI: 10.1021/am507428r
ACS Appl. Mater. Interfaces 2015, 7, 1257−1269

(41) Guo, Z.; Liu, B.; Zhang, Q.; Deng, W.; Wang, Y.; Yang, Y. Recent Advances in Heterogeneous Selective Oxidation Catalysis for Sustainable Chemistry. *Chem. Soc. Rev.* **2014**, *43*, 3480−3524.
(42) Wang, C.; Zhang, H.; Li, F.; Zhu, L. Degradation and Mineralization of Bisphenol A by Mesoporous Bi_2WO_6 under Simulated Solar Light Irradiation. *Environ. Sci. Technol.* **2010**, *44*, 6843−6848.
(43) Sheng, J.; Li, X.; Xu, Y. Generation of H_2O_2 and OH Radicals on Bi_2WO_6 for Phenol Degradation under Visible Light. *ACS Catal.* **2014**, *4*, 732−737.
(44) Saison, T.; Gras, P.; Chemin, N.; Chanéac, C.; Durupthy, O.; Brezová, V.; Colbeau-Justin, C.; Jolivet, J.-P. New Insights into Bi_2WO_6 Properties as a Visible-Light Photocatalyst. *J. Phys. Chem. C* **2013**, *117*, 22656−22666.
(45) Stacchiola, D. O.; Burkholder, L.; Tysoe, W. T. Enantioselective Chemisorption on a Chirally Modified Surface in Ultrahigh Vacuum: Adsorption of Propylene Oxide on 2-Butoxide-Covered Palladium (111). *J. Am. Chem. Soc.* **2002**, *124*, 8984−8989.
(46) Wang, Q.; Zhang, M.; Chen, C.; Ma, W.; Zhao, J. Photocatalytic Aerobic Oxidation of Alcohols on TiO_2: The Acceleration Effect of a Brønsted Acid. *Angew. Chem., Int. Ed.* **2010**, *49*, 7976−7979.
(47) Liang, S.; Wen, L.; Lin, S.; Bi, J.; Feng, P.; Fu, X.; Wu, L. Monolayer HNb_3O_8 for Selective Photocatalytic Oxidation of Benzylic Alcohols with Visible Light Response. *Angew. Chem., Int. Ed.* **2014**, *53*, 2951−2955.
(48) Qamar, M.; Elsayed, R. B.; Alhooshani, K. R.; Ahmed, M. I.; Bahnemann, D. W. Chemoselective and Highly Efficient Conversion of Aromatic Alcohols into Aldehydes Photocatalyzed by Ag_3PO_4 in Aqueous Suspension under Simulated Sunlight. *Catal. Commun.* **2015**, *58*, 34−39.

DOI: 10.1021/am507428r
ACS Appl. Mater. Interfaces 2015, 7, 1257−1269